J. Fluid Mech. (1966), *vol.* 26, *part* 3, *pp.* 481–506
Printed in Great Britain

Turbulent boundary layers in decreasing adverse pressure gradients

By A. E. PERRY
Department of Mechanical Engineering, University of Melbourne

(Received 25 March 1966)

The results of a detailed mean velocity survey of a smooth-wall turbulent boundary layer in an adverse pressure gradient are described. Close to the wall, a variety of profiles shapes were observed. Progressing in the streamwise direction, logarithmic, $\frac{1}{2}$-power, linear and $\frac{3}{2}$-power distributions seemed to form, and generally each predominated at a different stage of the boundary-layer development. It is believed that the phenomenon occurred because of the nature of the pressure gradient imposed (an initially high gradient which fell to low values as the boundary layer developed) and attempts are made to describe the flow by an extension of the regional similarity hypothesis proposed by Perry, Bell & Joubert (1966). Data from other sources is limited but comparisons with the author's results are encouraging.

1. Introduction

In this paper attempts are made to establish a correlation scheme for the mean velocity distributions in turbulent boundary layers which are developing in arbitrary adverse pressure gradients. The paper is concerned primarily with the case where the gradient is decreasing with streamwise distance.

Because of the encouraging success of the 'regional similarity' approach proposed by Perry *et al.* (1966), it was decided to see if it could be extended to a description of the new phenomena reported here. In this approach dimensional methods are used and, like many similar approaches, it fails to provide immediately obvious physical explanations of the phenomena. However, it appears to be a useful tool for sorting out the significant variables in the problem if it is used in conjunction with carefully measured data. Simple similarity equations are produced which can be checked readily by experiment. Such likely similarity laws would perhaps be overlooked when using methods of analysis based on preconceived ideas about the interaction of the turbulence with the mean flow. Analyses based on physical arguments could prove more fruitful once the likely governing parameters have been established and an attempt at such an analysis is shown later in the paper.

The usual theories of wall turbulence give the form of the mean-velocity distribution close to the wall by assuming that the gradient of this distribution at a point in the flow is related directly to the local shear stress τ at that point. Such theories are exemplified by Prandtl's mixing-length hypothesis or other theories which are consistent with the Boussinesq concept. The local shear stress

is determined by the use of the mean-flow momentum equation, and it is often assumed that close to the wall the mean-flow inertia forces are small. The distribution of local shear stress then becomes linear and is given by

$$\tau/\rho = (\tau_0/\rho) + \alpha y,$$

where τ_0 is the wall shear stress, ρ is the fluid density, α is the kinematic pressure gradient ($= (1/\rho)(dp/dx)$ where p is the static pressure and x is the streamwise distance) and y is the distance normal to the wall.

For the case when $\tau_0/\rho \gg \alpha y$, the effect of α can be ignored and these theories predict the logarithmic distribution of mean velocity U with y for flow beyond the viscous sublayer. For the case when $\alpha y \gg \tau_0/\rho$, the effect of τ_0 can be ignored and a $\frac{1}{2}$-power distribution in velocity is obtained. Hence the more general expression obtained by such analyses asymptotes to a logarithmic law for low values of y and approaches a $\frac{1}{2}$-power law for large values of y, and the theories indicate that these two laws are separated by a large blending region (e.g. see Townsend 1961, and Perry *et al.* 1966). The assumption that the mean relative motions at a point in the flow are governed by some property of the turbulence characteristic to that point (e.g. the Reynolds stress in the case of the momentum transfer theory) will be referred to as the 'local similarity hypothesis'.

Perry *et al.* (1966) in their regional similarity approach propose that the momentum equation is not directly relevant for determining the mean profile close to the wall provided the appropriate similarity parameters are used. Coles (1955) adopted this philosophy when considering the 'law of the wall', where he assumed that this law retained its universality irrespective of the state of balance of momentum. The momentum and continuity equation can then be used for finding the consequent shear-stress distribution and streamline pattern once the similarity law is known. In any case, if the variations of τ_0 and α are not too rapid, their local streamwise values will be sufficient for describing the profiles, and the mean velocity U is a function only of U_τ, α, ν and y, even if there are appreciable mean-flow accelerations present. U_τ is the shear velocity ($= (\tau_0/\rho)^{\frac{1}{2}}$) and ν is the kinematic viscosity. Regions which can be described in terms of the local streamwise values of the parameters will be regarded as belonging to the wall region. Beyond this region is the 'historical region' where such parameters are probably inadequate for describing the flow.

In this approach it is further assumed that there exist finite regions (which may be small or large) within which the profile shape can be described in terms of one characteristic regional parameter. This will be referred to as the 'regional similarity hypothesis'.

Adjacent to the wall there is a viscous region where both ν and U_τ govern the profile shape. However, beyond this is the fully turbulent region where it is proposed that U_τ alone is the governing regional parameter and so

$$\partial U/\partial y = \psi[y, U_\tau].$$

Dimensional analysis gives

$$\partial U/\partial y = U_\tau/(\mathscr{K} y),$$

where $\mathscr{K}$ is a universal constant. Integration leads to the logarithmic distribution. Further from the wall the appropriate parameters are U_τ and α and no analytical

deduction can be made by dimensional analysis alone since too many variables are involved. Such regions will be referred to as 'blending regions'. Finally, a region is encountered where only α plays a part and so

$$\partial U/\partial y = \tfrac{1}{2}K_1\alpha^{\frac{1}{2}}/y^{\frac{1}{2}},$$

where K_1 is a universal constant. Integration leads to the $\frac{1}{2}$-power equation.

The local similarity hypothesis predicts the same general behaviour. However, the regions are approached asymptotically and the effects of the parameters U_τ and α predominate over each other only in those regions where one makes a dominant contribution to the local shear stress, i.e. when τ_0/ρ is much greater or much less than αy. The regional similarity approach makes no such commitments and in fact the data cited by Perry *et al.* indicate that a logarithmic region extends out from the wall where αy is 1·41 times the value of τ_0/ρ, while the $\frac{1}{2}$-power region extends down to values near this. The solutions to the various differential equations for the velocity distribution, shown above, involves a treatment of the boundary conditions by a matching technique based on dimensional analysis. In this treatment the unknown variations of the velocity distribution in a blending region can be accounted for by one empirical universal constant and an example of this is shown in §4.

In the local similarity approaches the variations of velocity in the blending regions are given and this variation governs the value of the constant involved in the asymptotic $\frac{1}{2}$-power expression. Perry *et al.* have found this constant to disagree with experiment.

The final expressions and empirical constants obtained by the regional similarity approach have been found valid for the data cited by Perry *et al.* even when there were appreciable accelerations close to the wall. Further confirmation is given in this paper.

Subsequent experiments with adverse-pressure-gradient turbulent boundary layers have been carried out by the author. Other profile shapes besides the logarithmic and $\frac{1}{2}$-power forms were observed in regions close to the wall. The author believes that this was because of the nature of the pressure distribution used and possible extensions of the regional similarity hypothesis for describing these profile shapes are outlined. The data from other sources is compared with the author's results. This data is limited but agreement is encouraging.

2. Description of experiment

A flat vertical plate was installed in the working section of the wind tunnel at the University of Melbourne. This tunnel is a return-circuit type and has a basic cross section of octagonal form. Figure 1 is a diagrammatic representation of the working section and plate, and the major dimensions are shown. It can be seen that the plate is at an angle of attack to the approaching flow and the pressure distribution obtained is somewhat similar to that in a straight-wall diffuser. The purpose of the blister shown at the downstream end of the working section

was to remove separation on the plate, and the flap shown was installed to modify the flow near the leading edge so as to avoid separation bubbles.

The plate spanned the full height of the tunnel and felt seals were provided to isolate the flows on either side. Corner fillets, particularly at the leading edge, were found to be essential to remove separation on the floor and ceiling of the working section. Once separation occurred anywhere, the tunnel velocity

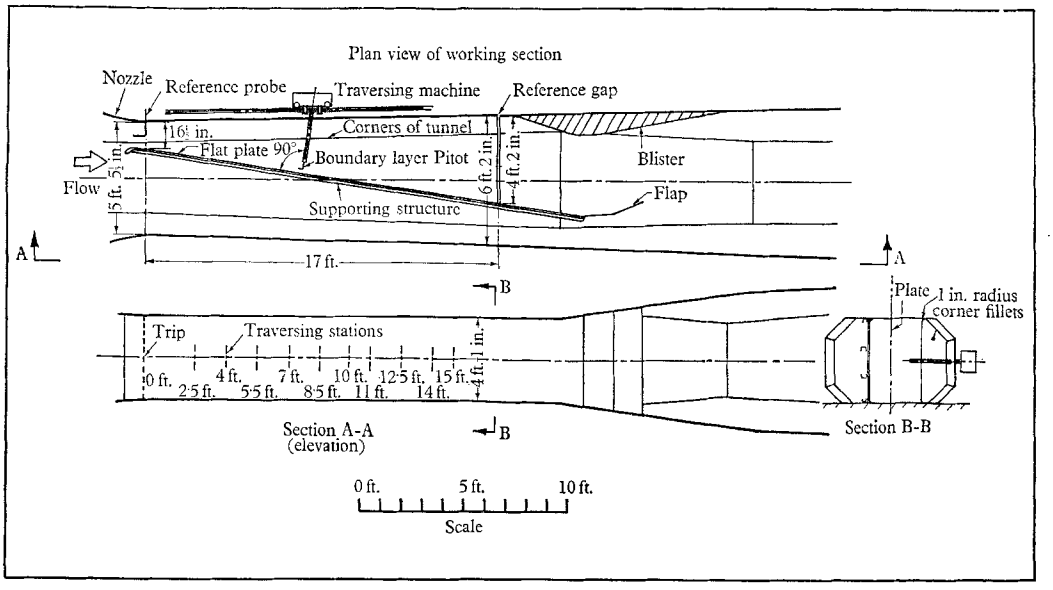

FIGURE 1. Diagrammatic representation of working section and plate.

fluctuated violently and the flow became largely three dimensional near the separation zones if these zones occurred on the floor and ceiling. Without separation, the flow was found to be reasonably steady and two dimensional, even in the corner regions. This latter point was checked with dye streaks and tufts. The turbulence level in the working section was reduced from approximately 1 % (without screens) to 0·3 % by the use of screens.

The pressure recovery was quite large and a fairly detailed plot of the pressure distribution is shown in figure 2. Fifteen feet of the plate were traversed along its centre line and the boundary layer was found to be approximately 16 in. thick at the 15 ft. station.

The nominal Reynolds number of the flow (based on the velocity U_0 indicated by the reference probe shown in figure 1) was $9{\cdot}23 \times 10^5 \text{ft.}^{-1}$, and this varied slowly by approximately $\pm \frac{1}{2}$ % during each mean velocity traverse. The tunnel speed was held reasonably constant at about 145 ft./sec but this varied from traverse to traverse by ± 2 %. However, taking into account the temperature variations, the maximum variation in the reference Reynolds number was only ± 1 % between traverses. All pertinent data is shown in table 1.

Ten very detailed mean velocity traverses were made (up to 60 points for some profiles) using an automatic traversing and plotting system developed by the author for work of this kind. The traversing system could be programmed to

take measurements at desired increments of y and pause for the readings to settle. Non-dimensional velocity was plotted automatically against log y with the use of a recorder, function generator and normalizing system. The traver-

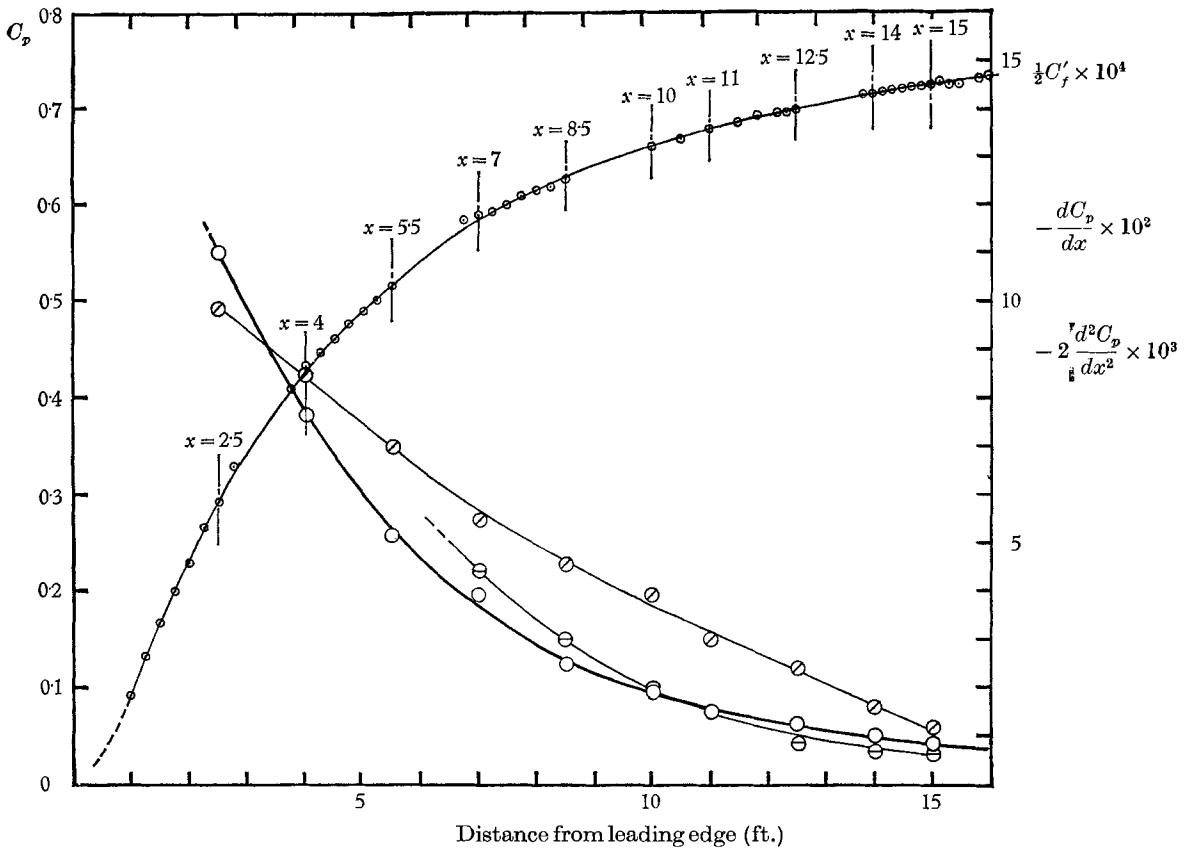

FIGURE 2. Distribution of the various parameters. ⊙, Pressure coefficient C_p; ○, $(dC_p/dx) \times 10^2\,\text{ft.}^{-1}$; ⊖, $2(d^2C_p/dx^2) \times 10^3\,\text{ft.}^{-2}$; ∅, $\frac{1}{2}C_f' \times 10^4$. Vertical lines indicate stations where mean velocity profiles were measured.

x ft.	U_0 (ft./sec)	C_p	$-\frac{dC_p}{dx} \times 10^2$ (ft.$^{-1}$)	$-\frac{d^2C_p}{dx^2} \times 10^3$ (ft.$^{-2}$)	$C_f' \times 10^4$	$\frac{U_0}{\nu} \times 10^{-5}$
2·5	147	0·292	11·0	6·75	19·8	9·26
4	145·5	0·43	7·66	4·7	17	9·21
5·5	143·5	0·515	5·15	3·0	14	9·26
7	146	0·589	3·91	2·2	10·9	9·20
8·5	143·7	0·626	2·50	1·5	9	9·17
10	147·5	0·66	1·96	1·0	7·8	9·20
11	147	0·679	1·56	0·75	6	9·24
12·5	143·5	0·698	1·28	0·425	4·8	9·20
14	146	0·716	1·05	0·35	3·10	9·20
15	148·7	0·733	0·85	0·32	2·37	9·36

TABLE 1

sing Pitot was connected to a Siemens† 144 mm 'Teleperm' differential pressure transducer with square-root action. The time lags in the system removed all fluctuations in the velocity indications on the recorder. A comparison of the non-dimensional velocity indicated on the recorder in a free stream test with that found using a Betz manometer and standard Prandtl tube gave a linearity within $\frac{1}{2}\%$ for most of the range of interest. The variation of static pressure through the boundary layer was found to be negligible. However, this was checked thoroughly only at the 10 ft. station. The pressures were measured by a probe which was positioned at 1 to 2 in. from the wall.

The repeatability of results was very encouraging and the lack of scatter in the velocity profiles was to prove to be of importance in the work outlined in this paper.

3. Correlation of experimental results with the logarithmic and half-power equations

By the use of the regional similarity hypothesis, it has been shown by Perry *et al.* that, provided the boundary layer is sufficiently developed, the regions shown in figure 3 occur where for the viscous region I

$$U/U_\tau = f[yU_\tau/\nu], \tag{1}$$

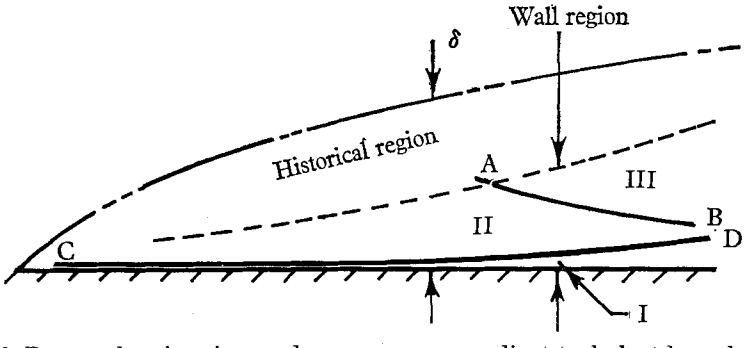

FIGURE 3. Proposed regions in an adverse-pressure-gradient turbulent boundary layer, after Perry *et al.* (1966).

and for region II, where $\partial U/\partial y$ is independent of ν,

$$\frac{U}{U_\tau} = \frac{1}{\mathscr{K}} \ln\left(\frac{yU_\tau}{\nu}\right) + A, \tag{2}$$

while for region III, where $\partial U/\partial y$ is independent of ν and U_τ, the velocity distribution is given by

$$\frac{U}{U_\tau} = K_1\left(\frac{\alpha y}{U_\tau^2}\right)^{\frac{1}{2}} + \frac{\Delta U_1}{U_\tau}\left[\frac{U_\tau^3}{\alpha\nu}\right], \tag{3}$$

where $\mathscr{K}$, K_1 and A are universal constants. $\Delta U_1/U_\tau$ will be referred to as the slip function and represents the non-dimensional velocity given by equation (3) if it is extrapolated to the wall. Square brackets are used throughout this paper

† The full-scale range of the transducer was continuously adjustable from 0 to 36 mm to 0 to 144 mm H_2O.

to denote a functional dependence. The complete derivation of these equations is not included here, since the steps and techniques are identical to those adopted in an extended development appearing later in the paper (also a complete derivation has been given by Perry *et al.*).

Regions II and III are separated by a blending region but it is very difficult to detect this from the data. The junction between equations (2) and (3) has been found by experiment to be almost tangential; that is, the curves join where $\partial U/\partial y$ given by each equation is the same. The locus of this junction is shown as line AB in figure 3. Line CD represents the outer boundary of the viscous region I. Dimensional reasoning shows that if the lines CD and AB are located at y_b and y_c respectively, then

$$y_b = M(\nu/U_\tau), \tag{4}$$

and

$$y_c = N(U_\tau^2/\alpha), \tag{5}$$

where M and N are universal constants. The value of M is about 30 while N has been found to be approximately 1·41.

Provided the boundaries CD and AB do not come too close to each other, a logarithmic region II should exist, and for this condition of flow it has been shown by Perry *et al.* that

$$\frac{\Delta U_1}{U_\tau} = \frac{1}{\mathscr{K}} \ln\left(\frac{CU_\tau^3}{\alpha\nu}\right) + A, \tag{6}$$

where C is a universal constant.

From an analysis of the experimental data of Schubauer & Klebanoff (1950), Perry & Joubert (1963) (rough wall), Johnston (1957, 1960) and of Perry *et al.* (1966), the numerical values of $K = 4{\cdot}16$ and $C = 0{\cdot}19$ were obtained. In obtaining these it was assumed that $\mathscr{K} = 0{\cdot}40$ and $A = 5{\cdot}1$.

The author's data has been plotted in the form U/U_1 *vs.* $\log_{10}(yU_1/\nu)$ in figure 4, (U_1 is the local free-stream velocity). Using the above numerical values, equation (2) can be put in the form

$$U/U_1 = 5{\cdot}76(\tfrac{1}{2}C_f')^{\frac{1}{2}} \log_{10}(yU_1/\nu) + 5{\cdot}76(\tfrac{1}{2}C_f')^{\frac{1}{2}} \log_{10}(\tfrac{1}{2}C_f')^{\frac{1}{2}} + 5{\cdot}1\,(\tfrac{1}{2}C_f')^{\frac{1}{2}}, \tag{7}$$

where C_f' is the local skin-friction coefficient (based on U_1). This equation is shown as a family of lines in figure 4 and from this the values of C_f' have been deduced.

This figure shows a fairly convincing verification of the 'logarithmic law of the wall'. A fairly smooth monotonic variation in C_f' resulted and this is shown in figure 2 and table 1.

Figure 5 shows the data plotted as U/U_1 *vs.* $y^{\frac{1}{2}}$ (in.$^{\frac{1}{2}}$) and equation (3) with equation (6) can be put into the form

$$U/U_1 = 4{\cdot}16(\alpha y/U_1^2)^{\frac{1}{2}} + 5{\cdot}76\,(\tfrac{1}{2}C_f')^{\frac{1}{2}} \log_{10}(0{\cdot}19U_\tau^3/\alpha\nu) + 5{\cdot}2(\tfrac{1}{2}C_f')^{\frac{1}{2}}, \tag{8}$$

using the above-mentioned numerical values. This equation is shown as a family of lines in figure 5 with the appropriate values of C_f' found from figure 4. α was found by graphical differentiation and a graph of dC_p/dx is shown in figure 2. The values are shown in table 1.

The correlation of results shown in figure 5 is quite satisfactory for many profiles but the extent of correlation diminishes as one proceeds downstream.

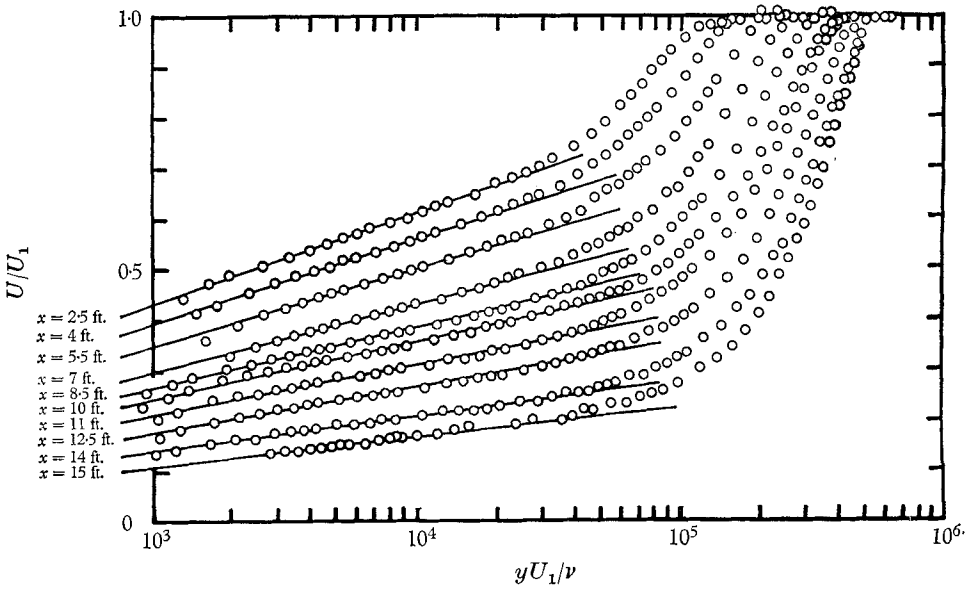

FIGURE 4. Correlation of results according to the logarithmic law of the wall (equation 7).

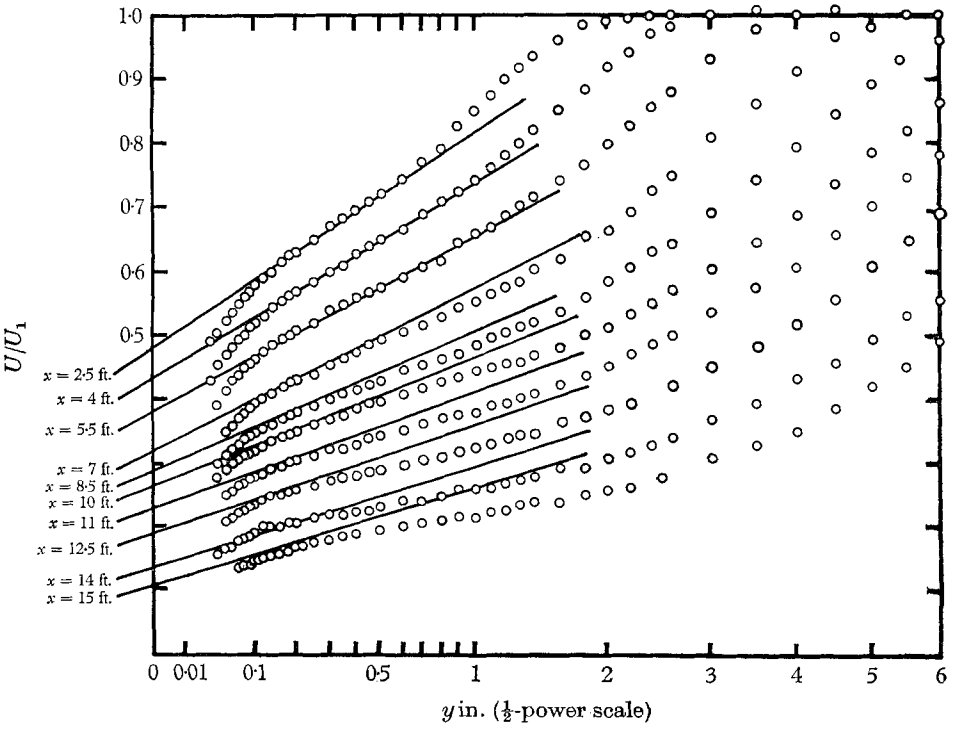

FIGURE 5. Correlation of results according to the $\frac{1}{2}$-power equation (equation 8).

Also, the slip function included in equation (8) appears to be a few per cent too high for many of the downstream profiles. The actual slip function of the profiles is shown plotted in figure 6 and is compared with the results obtained from other sources. The correlation is good and the value of $C = 0{\cdot}19$ is satisfactory although it should perhaps be slightly lower. The diminishing range of validity of the $\frac{1}{2}$-power equation was not observed in the experimental results cited by Perry *et al.* —in fact the results of Schubauer & Klebanoff and of Johnston showed extensive $\frac{1}{2}$-power regions to be applicable for profiles near to separation.

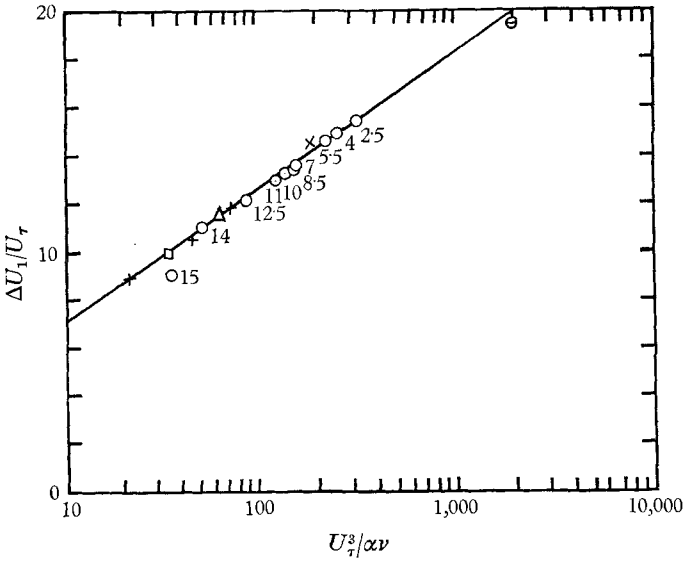

FIGURE 6. Slip function from present experiment and other sources. Line corresponds to equation (6). Numbers indicate distance in feet from the leading edge. ○, Author; ⊖, Perry & Joubert (1963) (rough wall); ×, Schubauer & Klebanoff (1950) ($x = 22{\cdot}5$ ft.); □, E. 2; △, E. 5 of Perry *et al.*; +, Johnston (1957, 1960). Plane-of-symmetry flow.

One plausible explanation of this departure in the author's experiment stems from a comparison of the pressure distributions used. In figure 7 the distribution used by Schubauer & Klebanoff (1950) can be seen to give a fairly constant pressure gradient α which is imposed over quite an extensive length of the boundary-layer development. A rapid fall-off in this gradient is seen near the separation region and this will be commented on later. The author's pressure distribution, on the other hand, shows an initially large α which then falls off to very low values as one proceeds downstream. Perhaps this means that the first derivative of the pressure has a diminishing influence while a new effect is entering. This effect could perhaps be associated with the second derivative of the pressure, which in this case has negative values. A profile in a region of decreasing pressure gradient may retain a 'memory' of higher upstream values of α and the second derivative is associated with these upstream values.

Figure 8 shows the pressure distribution used by Johnston. Here, the pressure gradient can be seen to be increasing as one proceeds downstream ($d\alpha/dx$ positive) and one can envisage the influence of upstream values of α being overridden

by an ever increasing local α. The $\frac{1}{2}$-power region found in Johnston's data extends almost throughout the whole boundary-layer thickness near separation (see Perry *et al.* 1966). It should be pointed out, however, that Johnston measured

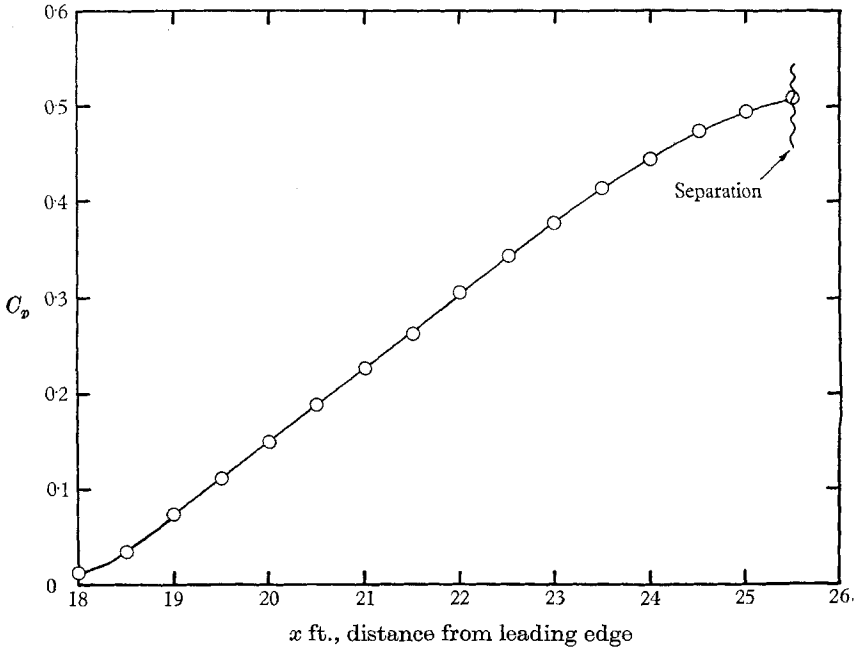

FIGURE 7. Pressure distribution in Schubauer & Klebanoff's (1950) experiments.

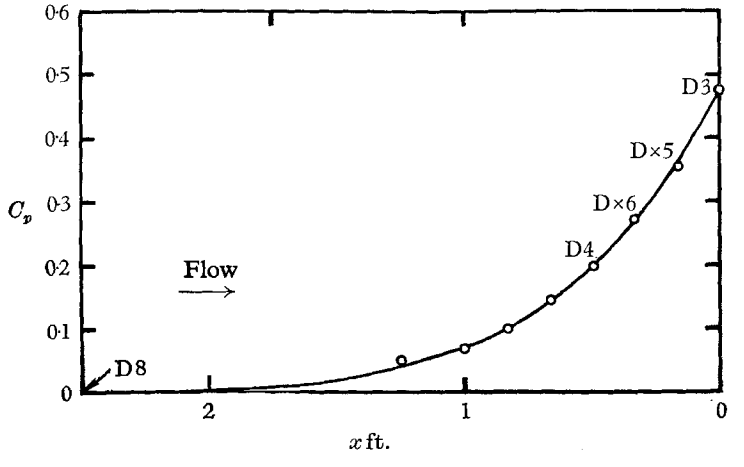

FIGURE 8. Pressure distribution of Johnston (1957).
(Plane of symmetry.)

his profiles along the plane of symmetry in a laterally diverging flow. All other results cited so far were from two-dimensional flows.

A noticeable difference between the author's results and those of Johnston is the persistence of an extensive logarithmic region in the former as one proceeds

down the plate. The line corresponding to AB in figure 3 is almost horizontal for the author's experiment. In Johnston's experiment, the $\frac{1}{2}$-power region penetrates into the logarithmic region and obliterates it before the boundary layer finally separates. This can be explained in terms of equations (4) and (5).

4. Possible extensions of the regional similarity hypothesis

From what could be described as 'local similarity reasoning' Stratford (1959*a*) indicated that possible departures from the $\frac{1}{2}$-power distribution could be explained in terms of the parameters $(\partial^2\tau/\partial y^2)_0$, etc., where the suffix 0 denotes the effective values at the wall. In view of earlier comments the author suggests instead that $(d\alpha/dx)$, $(d^2\alpha/dx^2)$, etc., should be used. Also, the values of these streamwise derivatives are constant throughout the whole boundary-layer thickness and could perhaps have a more direct bearing on the mean relative motions than quantities defined at the wall.

It is therefore tentatively proposed that beyond region III, shown in figure 3, there will emerge a new region, this region having its profile shape governed by the local streamwise value of $d\alpha/dx$ alone. The choice of $d\alpha/dx$ alone appears to be a logical extension of the findings of Perry *et al.* about the effects of the various parameters occurring separately in fairly isolated regions. This new region will be referred to as region IV and will be separated from region III by a blending region of unknown width. Perhaps region IV, given the right conditions, will penetrate into region III and obliterate it in much the same way as region III has been observed to penetrate into region II. Region IV will be regarded as belonging to the wall region, since it is still being described by local streamwise values of the appropriate quantity.

The velocity gradient in region IV will be given by

$$\partial U/\partial y = \phi[d\alpha/dx, y],$$

and dimensional analysis shows that

$$\partial U/\partial y = K_2(d\alpha/dx)^{\frac{1}{2}}, \tag{9}$$

where K_2 is a universal constant. However, the absolute mean velocity must be dependent on all of the variables involved in the wall region, that is,

$$U = \psi[y, U_\tau, \alpha, d\alpha/dx, \nu],$$

and dimensional analysis gives

$$\frac{U}{U_\tau} = \chi\left[\frac{y}{U_\tau}\left(\frac{d\alpha}{dx}\right)^{\frac{1}{2}}, \frac{U_\tau^3}{\alpha\nu}, \frac{\alpha}{U_\tau}\left(\frac{d\alpha}{dx}\right)^{-\frac{1}{2}}\right]. \tag{10}$$

From an integration of equation (9) and a comparison with equation (10), the following linear 'law' for the velocity distribution is obtained,

$$\frac{U}{U_\tau} = K_2\frac{y}{U_\tau}\left(\frac{d\alpha}{dx}\right)^{\frac{1}{2}} + \frac{\Delta U_2}{U_\tau}\left[\frac{U_\tau^3}{\alpha\nu}, \frac{\alpha}{U_\tau}\left(\frac{d\alpha}{dx}\right)^{-\frac{1}{2}}\right]. \tag{11}$$

It is implied in all equations that the higher derivatives of α are negative, and that $d\alpha/dx$, $d^2\alpha/dx^2$, etc., denote the moduli of the derivatives. $\Delta U_2/U_\tau$ is a slip function† analogous to that given in the $\frac{1}{2}$-power expression (equation 3).

The form of the function $\Delta U_2/U_\tau$ will be deduced for the case where a $\frac{1}{2}$-power region III exists. The simplest way of doing this is to assume that if the $\frac{1}{2}$-power equation and linear equation were extrapolated, their curves intersect at some value of y, y_d, say, and the effective velocity at this intersection is U_d. Of course the equations may not intersect, but a modified analysis gives the same result.

From the assumptions made about the variables governing the mean velocity gradients in regions III and IV, y_d depends on α and $d\alpha/dx$ alone. Dimensional analysis then gives

$$y_d = P\alpha(d\alpha/dx)^{-1},$$

where P is a universal constant. Substituting this into equations (3) and (11), two expressions for U_d are obtained. Equating these expressions enables the slip function to be obtained and final expression for the velocity distribution is

$$\frac{U}{U_\tau} = K_2\frac{y}{U_\tau}\left(\frac{d\alpha}{dx}\right)^{\frac{1}{2}} + E\frac{\alpha}{U_\tau}\left(\frac{d\alpha}{dx}\right)^{-\frac{1}{2}} + \frac{\Delta U_1}{U_\tau}\left[\frac{U_\tau^3}{\alpha\nu}\right], \tag{12}$$

where $E = \{K_1P^{\frac{1}{2}} - K_2P\}$ and is a universal constant. Hence, for this case

$$\frac{\Delta U_2}{U_\tau} = E\frac{\alpha}{U_\tau}\left(\frac{d\alpha}{dx}\right)^{-\frac{1}{2}} + \frac{\Delta U_1}{U_\tau}\left[\frac{U_\tau^3}{\alpha\nu}\right] \tag{13}$$

and if a logarithmic region exists then from equation (6)

$$\frac{\Delta U_2}{U_\tau} = E\frac{\alpha}{U_\tau}\left(\frac{d\alpha}{dx}\right)^{-\frac{1}{2}} + \frac{1}{\mathscr{K}}\ln\left(\frac{CU_\tau^3}{\alpha\nu}\right) + A. \tag{14}$$

The velocity profiles were plotted as U/U_1 *vs.* y and extensive linear variations were found to exist; these are shown in figure 9. The value of $d\alpha/dx$ was obtained by graphical differentiation (see table 1 and figure 2 for d^2C_p/dx^2) and it was found that equation (12) correlates quite well with most of the downstream profiles if the values $K_2 = 27{\cdot}3$, $E = 0{\cdot}105$ and the numerical values adopted in equations (7) and (8) are used. Equation (12), for the form of plotting adopted, then becomes

$$\frac{U}{U_1} = 27{\cdot}3\frac{y}{U_1}\left(\frac{d\alpha}{dx}\right)^{\frac{1}{2}} + 0{\cdot}105\frac{\alpha}{U_1}\left(\frac{d\alpha}{dx}\right)^{-\frac{1}{2}} + 5{\cdot}76\,(\tfrac{1}{2}C_f')^{\frac{1}{2}}\log_{10}\left(\frac{0{\cdot}19U_\tau^3}{\alpha\nu}\right) + 5{\cdot}1(\tfrac{1}{2}C_f')^{\frac{1}{2}}. \tag{15}$$

This equation is shown as the family of lines in figure 9 and it can be seen that the correlation of the lines with the data for both slope and intercept is quite remarkable. However, when one considers the probable inaccuracies in calculating $d\alpha/dx$, this degree of correlation may be fortuitous.

Equation (12) is a quadratic in $P^{\frac{1}{2}}$ and this implies that it is possible for the linear equation to intersect the $\frac{1}{2}$-power equation twice if the equations are extrapolated. From figure 9 it can be seen that this does in fact occur. The dotted line shown is the extrapolated $\frac{1}{2}$-power equation applicable to the profile at

† $\Delta U_2/U_\tau$ was used for the roughness function in the paper of Perry, Bell & Joubert (1966).

$x = 10$ ft. There appears to be some sort of blending zone between regions III and IV, and this is seen as a kink in the experimental plot between the two crosses shown in the figure for $x = 10$ ft.

For the purposes of simplicity, the centre of this blending region will be regarded as the junction between the two main regions, and dimensional analysis shows that its location y'_d is proportional to y_d. Therefore

$$y'_d = P'\alpha(d\alpha/dx)^{-1}, \tag{16}$$

and from an analysis of the data $P' \approx 0{\cdot}022$.

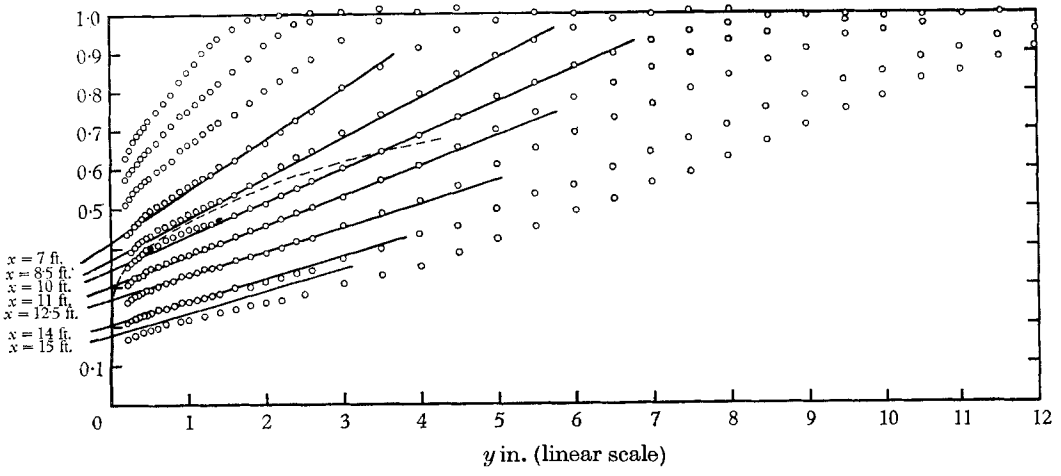

FIGURE 9. Correlation of results according to the linear equation (15). Broken curve represents extrapolated $\frac{1}{2}$-power equation for profile at $x = 10$ ft. The two crosses indicate limit of a possible blending zone in the same profile.

The various hypothetical loci which give the junctions between the various regions can now be mapped out according to equations (4), (5) and (16). Figure 10(*a*) shows the junctions given by y_c and y'_d. Although $\alpha^{\frac{1}{2}}$ and $(d\alpha/dx)^{\frac{1}{2}}$ can be evaluated with reasonable accuracy, the values of ratio $\alpha(d\alpha/dx)^{-1}$ are dubious. However, using these values it appears that the locus of y'_d is fairly horizontal. From this one would expect a linear region to appear in the profiles at $x = 2{\cdot}5$ ft., 4 ft. and 5·5 ft. The fact that it does not may perhaps be explained in terms of the degree of development of the boundary layer. The cross-hatched line shown in figure 10(*a*) represents a conjectured boundary between the wall region and historical region and, as the boundary layer develops, this wall region thickens. Beyond the wall region, local streamwise values of the parameters are not sufficient to describe the flow, but there could be, at certain stages of development, a considerable overlap between what is apparently the wall region and the historical region. This is indicated in the figure by the dotted lines. It is therefore proposed that a new region will not form until the length scale defining its lower junction or boundary is less than the thickness of the wall region. Figure 10(*b*) represents some hypothetical situation which illustrates the point a little better.

The value of y'_d near the back of the plate appears to be rising rapidly (if one can trust the accuracy of the calculations). This would imply an increasing width of the $\frac{1}{2}$-power region which in fact does not occur. On closer examination of

figure 9, the last few downstream profiles appear to be showing a diminishing linear region and that yet another effect appears to be penetrating into the wall region. Following the pattern which has emerged from regions II, III and IV where the velocity gradients are proportional to y^{-1}, $y^{-\frac{1}{2}}$ and y^0 respectively, perhaps yet another region with velocity gradients proportional to $y^{\frac{1}{2}}$ may exist.

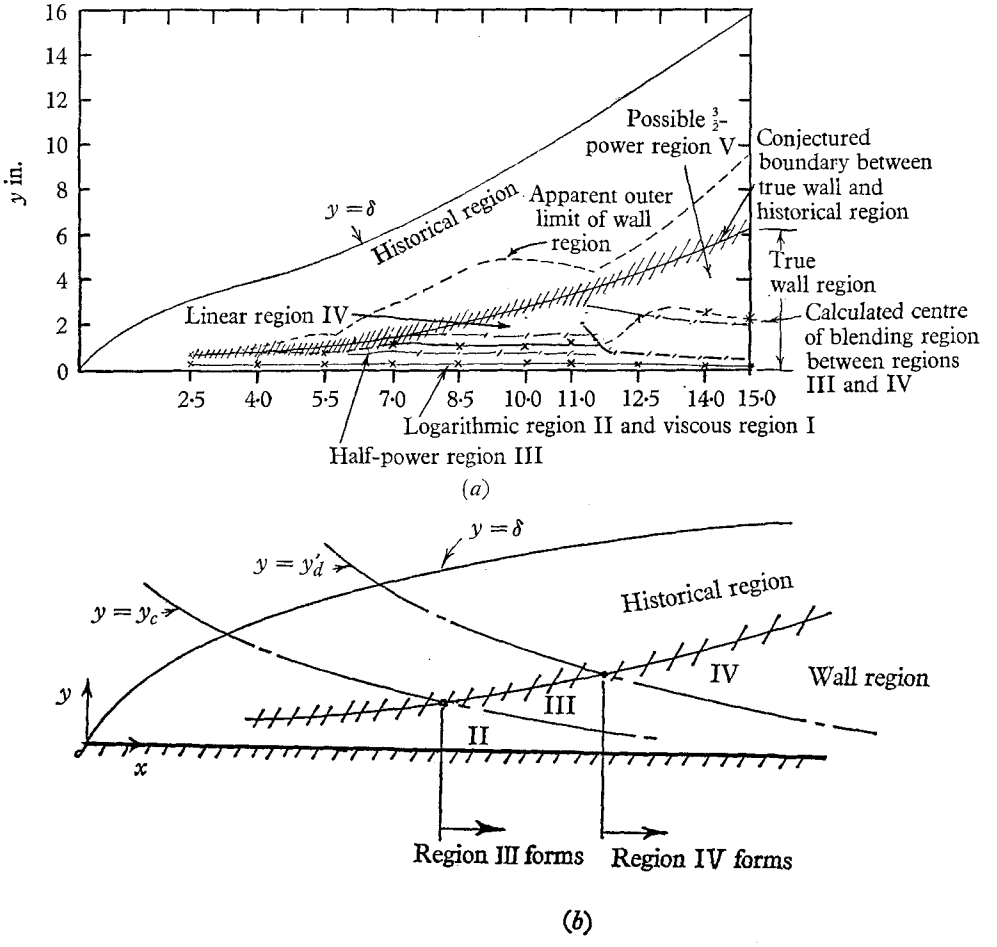

FIGURE 10. (*a*) Calculated and conjectured boundaries of various regions. ×, Calculated; –/–/–/–, conjectured limits of blending regions. (*b*) Diagram showing possible effect of boundary-layer history on the formation of a new region.

This would give a region V with a $\frac{3}{2}$-power distribution of velocity and could perhaps be explained in terms of the derivative $d^2\alpha/dx^2$. This region, with its associated blending region may be penetrating into the $\frac{1}{2}$-power region. The linear region for the last three downstream profiles may not really exist.

Figure 11 shows the velocity profiles plotted according to U/U_1 *vs.* $y^{\frac{3}{2}}$ and extensive linear plots can be seen to occur in the last downstream profiles at $x = 12{\cdot}5$, 14 and 15 ft. A regional similarity analysis would show that

$$\frac{U}{U_\tau} = K_3 \frac{y^{\frac{3}{2}}}{U_\tau}\left(\frac{d\alpha}{dx}\right)^{\frac{1}{2}} + \frac{\Delta U_3}{U_\tau}\left[\frac{U_\tau^3}{\alpha\nu}, \frac{\alpha}{U_\tau}\left(\frac{d\alpha}{dx}\right)^{-\frac{1}{2}}, \frac{1}{\alpha^{\frac{1}{2}}}\left(\frac{d\alpha}{dx}\right)\left(\frac{d\alpha^2}{dx^2}\right)^{-\frac{1}{2}}\right], \tag{17}$$

where K_3 is a universal constant. However, because of the difficulty in obtaining reliable values of $d^2\alpha/dx^2$ and considering the lack of sufficient number of profiles, no attempt was made to evaluate any of the constants involved. A method which may show promise if there were sufficient profiles would be to assume that equation (17) is valid, and from the profiles deduce $K_3\,(d^2\alpha/dx^2)^{\frac{1}{2}}$. This could be integrated and compared with the reasonably accurate distribution of $d\alpha/dx$. If a curve of the required shape were to be produced, this would be further evidence for the validity of equation (17) and K_3 could be evaluated.

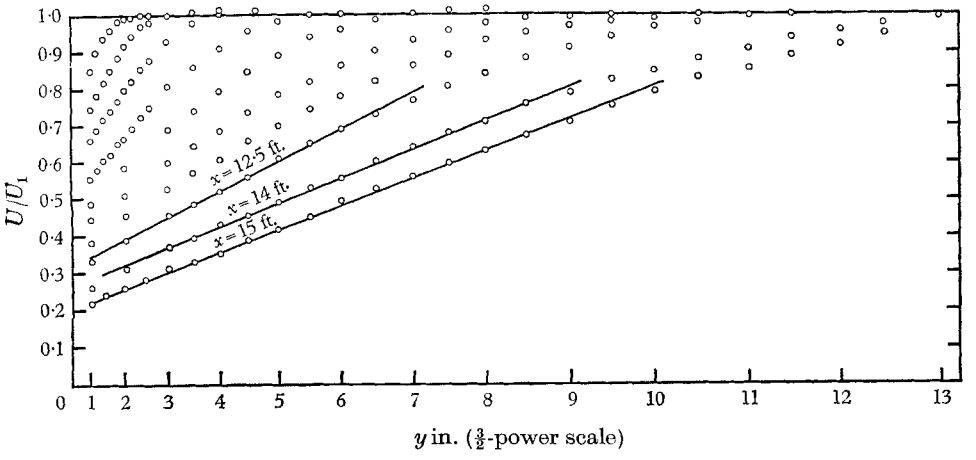

FIGURE 11. Conjectured $\frac{3}{2}$-power distribution in velocity.

If the $\frac{3}{2}$-region joined into a linear region (it does not appear so in this experiment), the junction and hence the centre of the associated blending zone would be given by

$$y'_e = Q'(d\alpha/dx)\,(d^2\alpha/dx^2)^{-1}, \tag{18}$$

where Q' is a universal constant.

5. Boundary-layer separation and criteria for the existence of various regions

From what has been observed it can be concluded that boundary-layer separation does not appear to be associated with a single universal profile shape (as in the case of Coles's law of the wake; Coles 1956) and any criteria for separation must take into account a multitude of possible behaviours. It is conjectured here that if the regions I, II, III and IV exist simultaneously, then they will continue to exist provided $y_b < y_c < y'_d < y'_e$, that is

$$M\nu/U_\tau < NU_\tau^2/\alpha < P'\alpha(d\alpha/dx)^{-1} < Q'\,(d\alpha/dx)\,(d^2\alpha/dx^2)^{-1}. \tag{19}$$

If any two adjacent terms in the above expression approach each other in value then the associated blending regions will coalesce and the appropriate region will be obliterated. If any two adjacent terms contradict the above inequality then new lengths defining the position of the various junctions can be deduced by the methods outlined in this paper. It may be possible, for example, for a linear region to join on to a logarithmic region. This has been found to be likely in the data of von Kehl (1943).

II(U_τ)	III(α)	IV $\left(\frac{d\alpha}{dx}\right)$	$V\left(\frac{d^2\alpha}{dx^2}\right)$	←Regions ↓
$y_{12} = A_{12}\frac{\nu}{U_\tau}$	$y_{13}^* = A_{13}^*\frac{\nu^{\frac{2}{3}}}{\alpha^{\frac{1}{3}}}$	$y_{14}^* = A_{14}^*\nu^{\frac{1}{2}}\left(\frac{d\alpha}{dx}\right)^{-\frac{1}{4}}$	$y_{15}^* = A_{15}^*\nu^{\frac{2}{5}}\left(\frac{d^2\alpha}{dx^2}\right)^{-\frac{1}{5}}$	$I\,(\nu, U_\tau)$ for y_{12} or (ν, α) for y_{13}^* or $\left(\nu, \frac{d\alpha}{dx}\right)$ for y_{14}^* or $\left(\nu, \frac{d^2\alpha}{dx^2}\right)$ for y_{15}^*
	$y_{23} = A_{23} = \frac{U_\tau^2}{\alpha}$	$y_{24} = A_{24}U_\tau\left(\frac{d\alpha}{dx}\right)^{-\frac{1}{2}}$	$y_{25} = A_{25}U_\tau^{\frac{2}{3}}\left(\frac{d^2\alpha}{dx^2}\right)^{-\frac{1}{3}}$	II (U_τ)
		$y_{34} = A_{34}\alpha\left(\frac{d\alpha}{dx}\right)^{-1}$	$y_{35} = A_{35}\alpha^{\frac{1}{2}}\left(\frac{d^2\alpha}{dx^2}\right)^{-\frac{1}{2}}$	III(α)
			$y_{45} = A_{45}\left(\frac{d\alpha}{dx}\right)\left(\frac{d^2\alpha}{dx^2}\right)^{-1}$	IV $\left(\frac{d\alpha}{dx}\right)$

TABLE 2. Various length scales associated with region boundaries.

The criteria for the existence of regions other than the simple case represented by expression (19) could become quite complex, since many more possible lengths are involved. It is difficult to decide on the conditions in which these lengths have a meaning or importance without further clues from experiment (although many conjectures could be made). For completeness, these lengths are listed in table 2. This tabulation lends itself to a more general notation, e.g. a length which gives the distance from the wall to the place where a logarithmic region II and linear region IV join, is y_{24} and dimensional analysis gives this as $A_{24}U_\tau(d\alpha/dx)^{-\frac{1}{2}}$, where A_{24} is a universal constant. Thus the various universal constants which have already been mentioned are

$$M \equiv A_{12}; \quad N \equiv A_{23}; \quad P' \equiv A_{34}, \quad \text{and} \quad Q' \equiv A_{45}.$$

The quantities with asterisks refer to the outer boundary of the viscous region for the case of zero skin friction. For non-zero values no deductions can be made by dimensional analysis alone since too many variables are involved. The quantities y^*_{14} and y^*_{15} probably do not have much meaning. The quantities in parenthesis after the Roman numerals are the appropriate regional parameters.

6. Comparison with other data

Other sources of data which show results similar to those reported here are Nikuradse (1929) (e.g. see Schlichting 1960), von Kehl (1943), Schubauer & Klebanoff (1950), Clauser (1954) and Stratford (1959*a*, *b*). The first two workers mentioned above measured boundary-layer profiles in straight-wall diffusers and these would give pressure gradients of the same type as those used by the author.

In Nikuradse's experiments, the diffuser angle was varied and for large angles linear regions appear to have formed. By replotting the data, $\frac{1}{2}$-power regions seem to be present for the smaller angles. For the larger angles the boundary layer was probably more developed. Figure 12 (*a*) shows the conjectured $\frac{1}{2}$-power regions while figure 12 (*b*) shows the possible linear regions.

The results of von Kehl show very extensive linear regions. However, due to lack of detailed pressure-gradient data in the above sources it was not considered worth while to attempt any numerical correlations.

As mentioned earlier, the pressure gradient of Schubauer & Klebanoff fell rapidly as separation was approached and so linear regions may perhaps be starting to form. Spence (1956) has plotted some of their profiles according to the logarithmic law of the wall and deduced some values for C'_f. By interpolating from a faired-in curve for C'_f the author has calculated the slip functions for the $\frac{1}{2}$-power equation for many of the profiles just upstream of separation using the numerical values of the constant given earlier (Perry *et al.* checked only the slopes on the $\frac{1}{2}$-power plot, except for the profile at $x = 22{\cdot}5$ ft. where the slip function was also checked). The correlation is shown in figure 13 and it can be seen that for the last downstream profiles the characteristic dip appears. There are an inadequate number of points to justify a linear region and this dip may be the associated blending region.

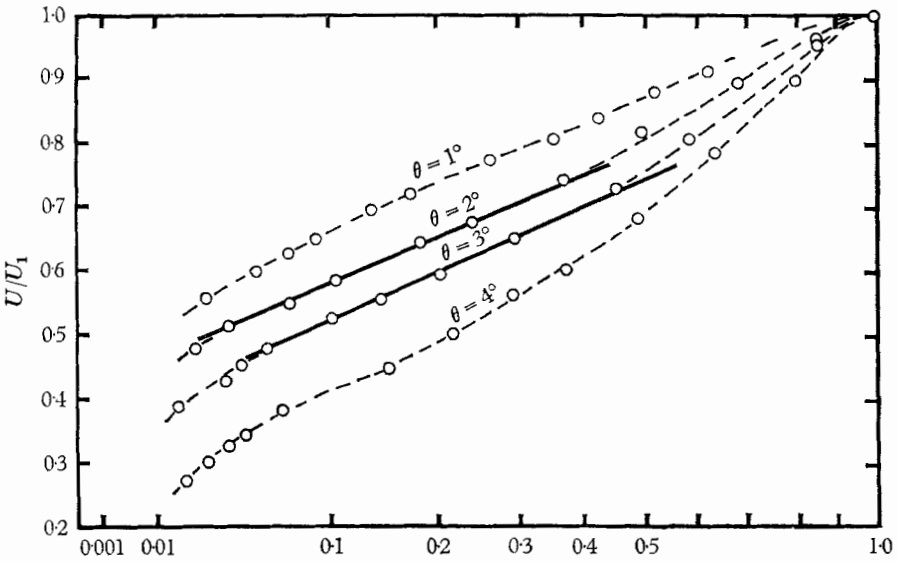

(*a*)

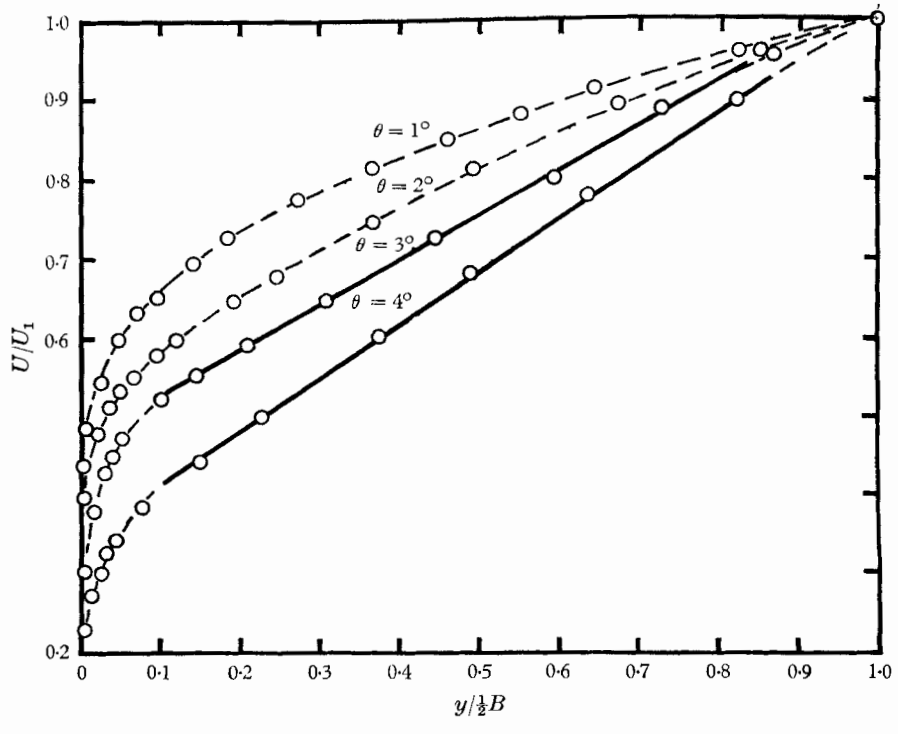

(*b*)

FIGURE 12. (*a*) Conjectured $\frac{1}{2}$-power regions in Nikuradse's data. θ is half the diffuser angle. (*b*) Conjectured linear regions in Nikuradse's data. ———, Conjectured regions; – – – –, curve of best fit.

The data of Clauser (1954) has been analysed in the same way. His pressure distributions 1 and 2 are shown in figure 14 and these are seen to have the same trend as the author's pressure gradients. Figure 15 shows the velocity profiles corresponding to distribution 1 correlated according to the $\frac{1}{2}$-power equation (8). The correlation is satisfactory except for the last few downstream profiles which exhibit the same trend as Schubauer & Klebanoff's results only more noticeably. (The theoretical slip function appears to be slightly low in these last downstream profiles).

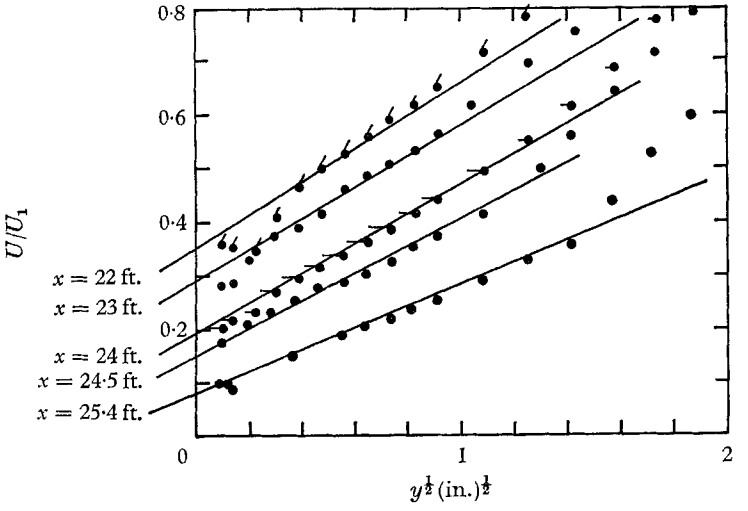

FIGURE 13. Comparison of Schubauer & Klebanoff's (1950) data with equation (8) using Spences's values of skin friction.

Pressure distribution 2 shows a much larger upstream gradient and lower downstream gradient. Also the boundary layer is twice as thick as in the previous case and so is probably more developed. No extensive $\frac{1}{2}$-power or logarithmic distributions were found due to the inadequate number of experimental points taken close to the wall. C_f' was determined by plotting the profiles on a Clauser chart (Clauser 1954) and a few points from each profile appear to be in a logarithmic region. C_f' was determined in the same way in the previous case but there the logarithmic regions were more apparent. Figure 16 shows the profiles compared with the linear equation (15) using the author's numerical values. The slip function was found by assuming the existence of a logarithmic and $\frac{1}{2}$-power region. The correlation of the results is fair except for the last few profiles where a $\frac{3}{2}$-region may perhaps be forming. The short vertical lines shown correspond to the calculated values of y_d' using $P' = 0{\cdot}022$. This has meaning only so long as a $\frac{1}{2}$-power and linear region exists and this may be the case for the upstream profiles. Figure 17 shows the profiles on a $\frac{3}{2}$ plot. The accuracy of the calculations of profile slope would be about $\pm 10\,\%$ for the upstream profiles and $\pm 20\,\%$ for the profiles far downstream. There is some uncertainty associated with Clauser's pressure distribution as quoted in his 1954 paper. It appears from his original data (only his profile data were available) that values of pressure were measured at a speed

slightly different from that used when the profiles were traversed and speeds between traverses differed. This has been corrected for by the author who assumed that the distribution of pressure coefficient was invariant with Reynolds number. The pressure gradients were calculated from an enlarged photograph of the published results and Clauser's faired-in curves were used.

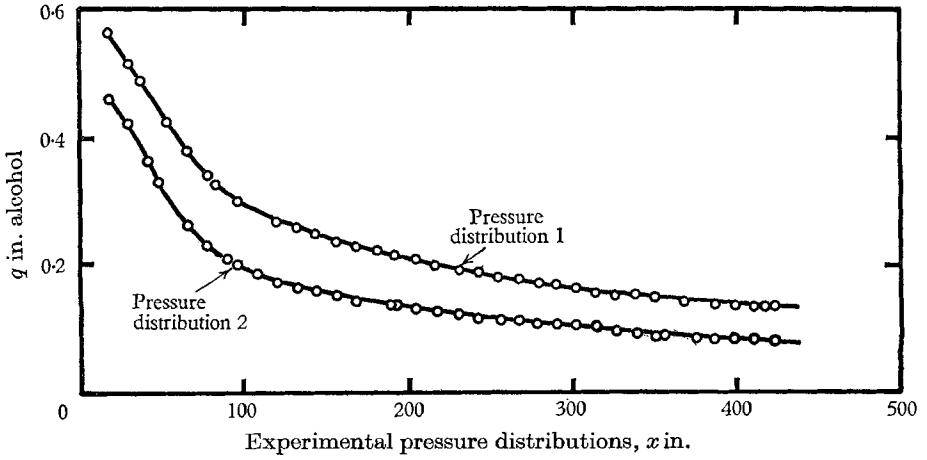

FIGURE 14. Clauser's pressure distributions 1 and 2.

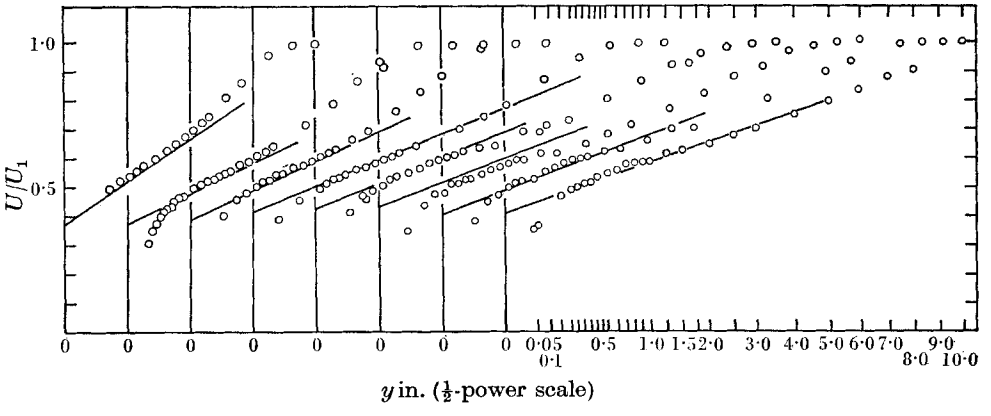

FIGURE 15. Comparison of Clauser's distribution 1 profiles with the $\frac{1}{2}$-power equation (8).

The data of Stratford (1959*b*) is shown in figure 18 for his first test series of profiles. Here the data is presented as U/U_0 *vs.* y, where U_0 is the velocity at a fixed reference station. Linear and possibly $\frac{3}{2}$-power regions appear to exist but it is difficult to tell whether $\frac{1}{2}$-power or logarithmic regions are present. Hence the slip functions for the linear equation could not be calculated. The lines shown correspond with the slope of the linear equation using the author's value of $K_1 = 27{\cdot}3$. The short vertical line in the figure shows a typical value of y'_d using the author's value of $P' = 0{\cdot}022$. Again, these calculations are fairly rough and the difficulty here was associated with the irregularities in Stratford's pressure distribution. It

is conjectured that the boundary layer does not respond to violent fluctuations in $d\alpha/dx$ and so a faired-in curve was used. Figure 19 shows the same profiles on a $\frac{3}{2}$ plot. Stratford's second test series shows a similar trend. The slope of one linear profile was checked by the author and the degree of correlation was about the same as for the previous series. Low curvatures in the pressure-distribution graph in this latter case made calculations of $d\alpha/dx$ difficult.

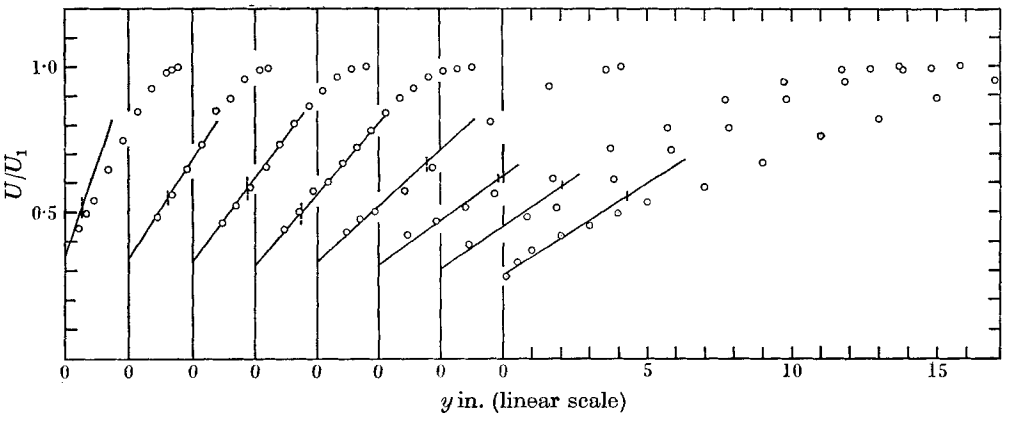

FIGURE 16. Comparison of Clauser's distribution 2 profiles with the linear equation (15).

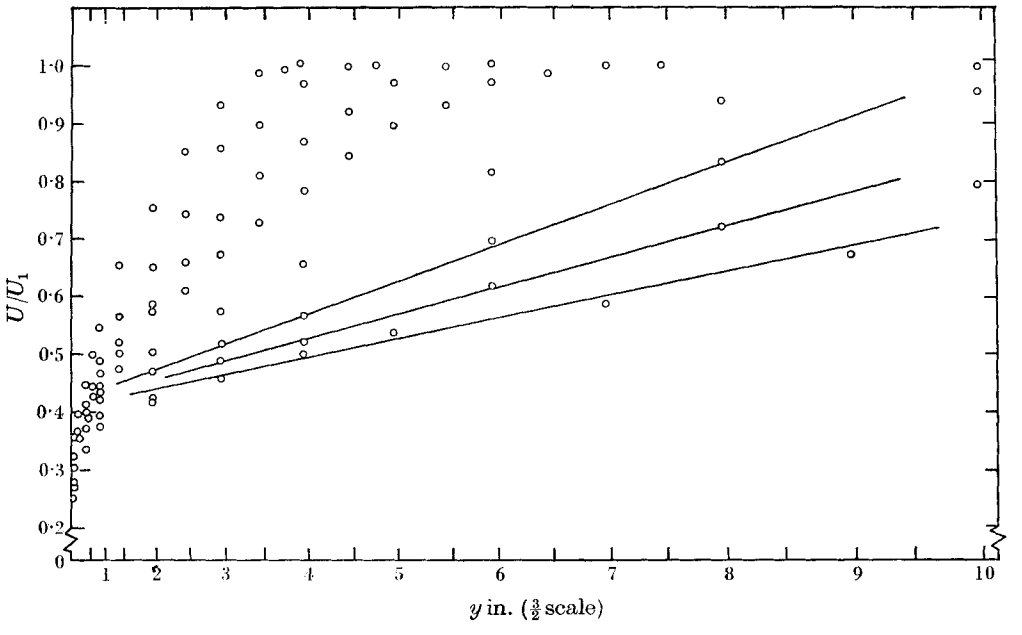

FIGURE 17. Clauser's distribution 2 profiles on a $\frac{3}{2}$ plot.
Lines represent conjectured $\frac{3}{2}$ region.

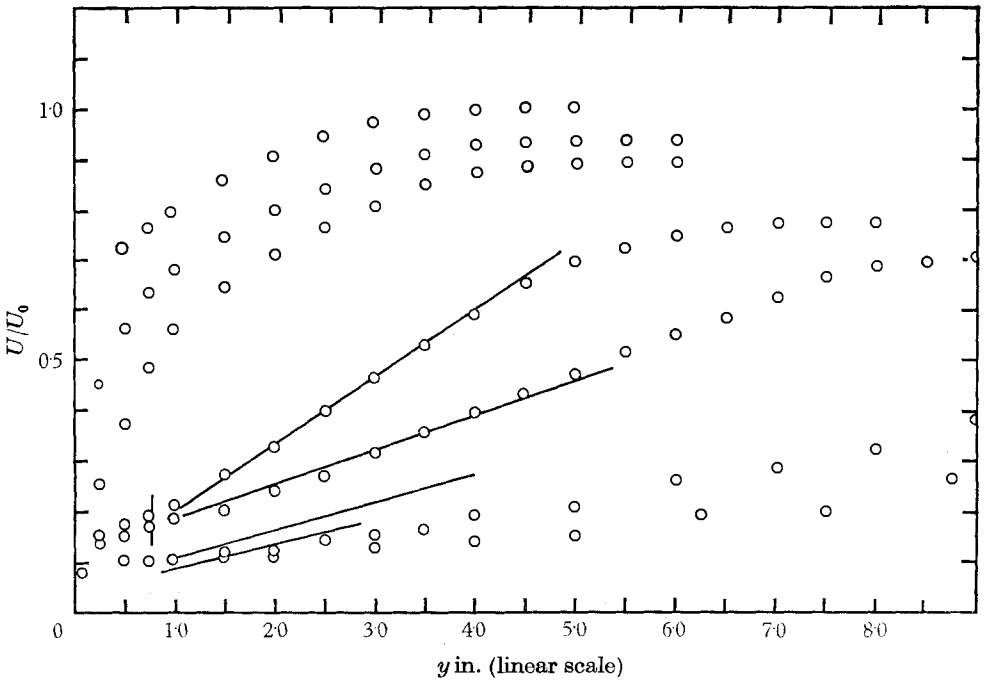

FIGURE 18. Stratford's first test series of profiles on a linear plot. Slope of lines correspond to author's value of $K_2 = 27{\cdot}3$.

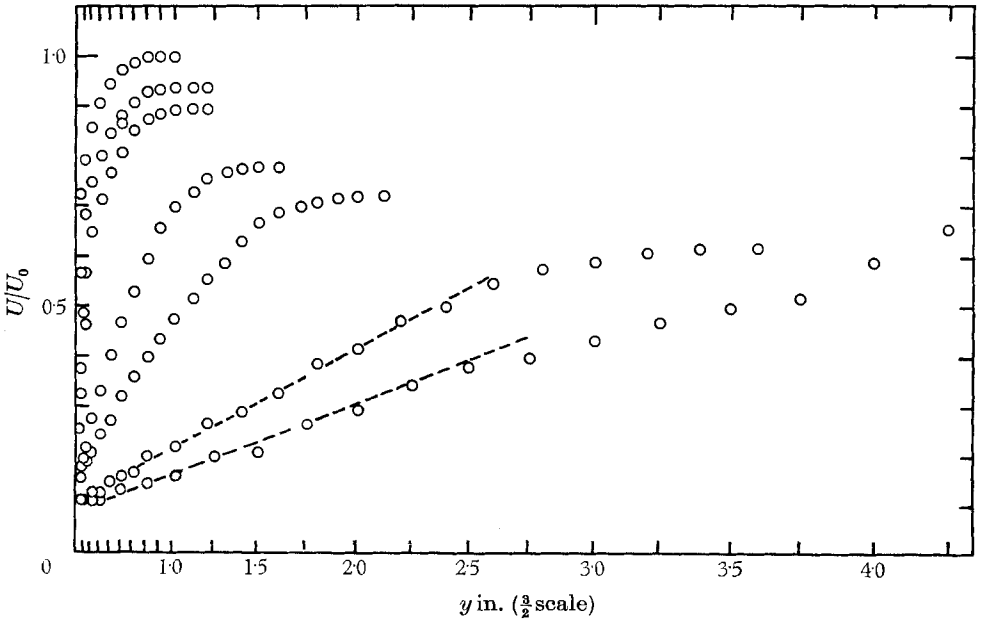

FIGURE 19. Stratford's first test series of profiles on a $\frac{3}{2}$ plot. Broken lines represent conjectured $\frac{3}{2}$ region.

7. A local similarity approach

A 'mixing-length' interpretation can be given to these results. Although the analysis is rather crude, it could perhaps lead to some insight into the physical processes occurring.

Assume that the fully-turbulent part of the wall region can be divided into two major zones.

In zone 1, which is closer to the wall, the equation which seems to describe the flow adequately is

$$\partial U/\partial y = U_\tau/\mathscr{K}y. \tag{20}$$

In zone 2 the appropriate equation is

$$\partial U/\partial y = \tfrac{1}{2}K_1\alpha^{\frac{1}{2}}/y^{\frac{1}{2}}. \tag{21}$$

This equation is applicable to the $\frac{1}{2}$-power region but it could perhaps be also applicable to the linear and $\frac{3}{2}$-power regions.

Consider a boundary layer which is developing in an adverse pressure gradient where $d\alpha/dx$ and $d^2\alpha/dx^2$ are negative. Close to the wall the fluid is moving slowly and so has plenty of time to adjust to the diminishing local streamwise values of α and equation (21) will be directly applicable. However, far from the wall the eddy structure may be coarser and the average vorticity is being convected more rapidly by the mean flow. These effects may possibly contribute to a 'time-lag' effect in the processes represented by equation (21). Perhaps for these regions the appropriate value of α to use is not that which prevails at the point of observation but one which would be measured at some effective distance l upstream where α is at some higher value α_R say. This 'persistence length' l is analogous to the length used in the usual mixing-length theories where some quantity or effect is conserved as the fluid element moves through a 'mixture length' l.

Hence the appropriate equation to use may be

$$\partial U/\partial y = \tfrac{1}{2}K_1\alpha_R^{\frac{1}{2}}/y^{\frac{1}{2}}. \tag{22}$$

The pressure gradient upstream of some station x can be expressed as a series expansion (ignoring terms higher than the third)

$$\alpha_R = \alpha + l\frac{d\alpha}{dx} + \tfrac{1}{2}l^2\frac{d^2\alpha}{dx^2}. \tag{23}$$

If in analogy with the usual mixing-length theories we let l be given by

$$l = \mathscr{K}'y, \tag{24}$$

where $\mathscr{K}'$ is a universal constant, then equations (22), (23) and (24) give

$$U = \frac{K_1}{2}\int\frac{1}{y^{\frac{1}{2}}}\left(\alpha + \mathscr{K}'y\frac{d\alpha}{dx} + \frac{\mathscr{K}'^2y^2}{2}\frac{d^2\alpha}{dx^2}\right)^{\frac{1}{2}}dy + C.$$

The function of integration C can be evaluated for the case when a $\frac{1}{2}$-power region exists by using the effective boundary condition

$$\left(\frac{U}{U_\tau}\right)_{y\to 0} = K_1\left(\frac{\alpha y}{U_\tau^2}\right)^{\frac{1}{2}} + \frac{\Delta U_1}{U_\tau}$$

and so

$$\frac{U}{U_\tau} = \frac{K_1}{2}\int_0^y\frac{1}{y^{\frac{1}{2}}}\left(\alpha + \mathscr{K}'y\frac{d\alpha}{dx} + \frac{\mathscr{K}'^2y^2}{2}\frac{d^2\alpha}{dy^2}\right)^{\frac{1}{2}}dy + \frac{\Delta U_1}{U_\tau}. \tag{25}$$

The various asymptotic forms of this equation agree with those forms deduced using the regional similarity hypothesis. For example, if

$$\alpha \ll \mathscr{K}' y \, d\alpha/dx \ll \tfrac{1}{2}\mathscr{K}'^2 y^2 d^2\alpha/dx^2,$$

that is, if $y \gg (1/\mathscr{K}')\,\alpha(d\alpha/dx)^{-1}$

and $y \ll (2/\mathscr{K}')\,(d\alpha/dx)\,(d^2\alpha/dx^2)^{-1},$ (26)

then (25) gives $$U/U_\tau = (\tfrac{1}{2}\mathscr{K}'^{\frac{1}{2}}K_1)\,y(d\alpha/dx)^{\frac{1}{2}} + (\Delta U_2'/U_\tau). \tag{27}$$

Expression (26) is analogous to the criterion

$$y_c < y < y_d'$$

found for the existence of a linear region when using the regional similarity approach. Equation (27) is identical to equation (11) if $\frac{1}{2}\mathscr{K}'^{\frac{1}{2}}K_1$ is put equal to K_2 and $\Delta U_2'/U_\tau$ is put equal to $\Delta U_2/U_\tau$.

With the author's value of $K_2 = 27{\cdot}3$, the value of $\mathscr{K}'$ and hence the 'persistence length' l is rather large; in fact it is too large to neglect the effect of the second derivative in the regions of the flow where the experiments indicate a linear profile. Also the blending region between the $\frac{1}{2}$-power and linear equations given by equation (25) does not correspond with the data and $\Delta U_2'/U_\tau$ is not equal to $\Delta U_2/U_\tau$. This appears to arise from an anomaly common to most mixing-length-type theories and could be explained in terms of the interpretation given to the length l. If it is taken as an effective length rather than an actual physical distance moved by a fluid element, then the actual distance moved could be much shorter than l. The fluid element does not then really know about the conditions too far upstream and as far as it is concerned, the derivative $d\alpha/dx$ can be regarded as constant over the effective distance l. The same difficulty is encountered in Prandtl's mixing-length hypothesis when considering a representative change in velocity of a fluid element as it moves from a slowly-moving layer to a rapidly-moving one. If these layers are at a distance l apart then this change Δu is usually taken as $\Delta u = l\,\partial U/\partial y$. This should be written as

$$\Delta u = l\frac{\partial U}{\partial y} + \tfrac{1}{2}l^2\frac{\partial^2 U}{\partial y^2} + \ldots$$

if l is interpreted as an actual length rather than an effective length.

The rather large blending regions given by equation (25) could be modified, by using a different expression for the variation of l, so that the equation agrees with experiment. Experiment indicates that on moving from the wall, l remains zero for some finite distance, then undergoes a fairly rapid increase and then settles down to a linear variation. This implies that a different eddy structure exists beyond the $\frac{1}{2}$-power region and the use of the regional similarity hypothesis seems a more suitable approach than this local similarity analysis. However, this latter approach could be a useful qualitative guide for gaining an understanding of the phenomena.

8. Possible applications to three-dimensional layers

Perry & Joubert (1965) have proposed a three-dimensional version of the law of the wall for a boundary layer which is yawed by a lateral component of the pressure gradient. The analysis was based essentially on eddy-viscosity concepts. From an analysis of Johnston's data (Johnston 1957), the proposed equation shows definite departures from the experimental data. Some preliminary attempts have been made to extend the regional similarity hypothesis to three-dimensional layers and this has met with some success. The details are in process of publication (Joubert, Perry & Brown 1966).

9. Conclusions

From the author's experiments and other data it appears that because of the nature of the gradient imposed on the flow, other profile shapes besides the logarithmic and $\frac{1}{2}$-power distributions are possible in the wall region. These profile shapes (a linear and $\frac{3}{2}$-power distribution) appear to fit in quite well with a more general version of the regional similarity hypothesis proposed by Perry *et al.* It seems that as the pressure gradient falls to small values, higher streamwise derivatives of the pressure become involved and the data indicate that their effects are confined to certain regions or layers in the flow and this gives rise to the linear and $\frac{3}{2}$-power regions. However, the experimental evidence for this latter region is very small.

To justify the proposed equations fully, more experiments should be carried out with particular care taken in measurement of the pressure distribution. These experiments should include the case of an increasing pressure gradient. Also the various turbulence quantities should be measured.

The author wishes to thank the Australian Institute of Nuclear Science and Engineering whose financial support made this project possible.

The author is also indebted to Professor F. H. Clauser and Dr B. S. Stratford who kindly supplied their original experimental data.

REFERENCES

CLAUSER, F. H. 1954 *J. Aero Sci.* **21**, 19.

COLES, D. 1955 50 *Jahre Grenzschichtforschung* (50 Years of Boundary Layer Research). H. H. Goertler and W. Tollmien (eds.). Braunschweig: Friedr. Viewey und Sohn.

COLES, D. 1956 *J. Fluid Mech.* **1**, 191.

JOHNSTON, J. P. 1957 Three dimensional turbulent boundary layer. Sc.D. Thesis, Massachusetts Institute of Technology.

JOHNSTON, J. P. 1960 *Trans. A.S.M.E.* Series D, **82**, 233.

JOUBERT, P. N., PERRY, A. E. & BROWN, K. C. 1966 To be published. Presented at General Motors Symposium, 'Fluid Mechanics of Internal Flows'.

VON KEHL, A. 1943 *Ingenieur Archiv.* **13**.

NIKURADSE, J. 1929 *VDI Forschungsarb* no. 289.

PERRY, A. E. & JOUBERT, P. N. 1963 *J. Fluid Mech.* **17**, 193.

PERRY, A. E. & JOUBERT, P. N. 1965 *J. Fluid Mech.* **22**, 285.

PERRY, A. E., BELL, J. B. & JOUBERT, P. N. 1966 *J. Fluid Mech.* **25**, 299.
SCHLICHTING, H. 1960 *Boundary Layer Theory*. New York: McGraw-Hill.
SCHUBAUER, C. B. & KLEBANOFF, P. S. 1950 *NACA TN* no. 2133.
SPENCE, D. A. 1956 *J. Aero. Sci.* **23**, 3.
STRATFORD, B. S. 1959*a* *J. Fluid Mech.* **5**, 1.
STRATFORD, B. S. 1959*b* *J. Fluid Mech.* **5**, 17.
TOWNSEND, A. A. 1961 *J. Fluid Mech.* **11**, 97.